AR-005-713

④

A BASIS FOR MODELLING CERAMIC COMPOSITE ARMOUR DEFEAT

Raymond L. Woodward

ABSTRACT

This work takes some of the major features of ceramic composite armour
failure, viz. fracture conoid formation, dishing failure of thin backing
plates, perforation failure of thick backing plates, and projectile erosion,
and by lumping masses to treat material acceleration simple models are
developed which allow computations on ceramic targets with both thin and
thick metallic backings. Two computer programs for these problems, CEP
and ECS, are documented, and calculations compared with a broad range of
empirical data and also used to discuss aspects of the interaction of
penetrators with ceramic composite armours. The good correlation of
models with experiment demonstrates the usefulness of the present
approach for studying ceramic composite armour defeat.

89 11   034

Approved for public release

CONTENTS

A BASIS FOR MODELLING CERAMIC COMPOSITE
ARMOUR DEFEAT

1. INTRODUCTION

The development of ceramic composite armours rests soundly on the basis of the work of Wilkins et al. [1-3] who developed the commonly used configuration of ceramic tiles supported by a thin ductile backing material. Wilkins used the HEMP finite difference computer code to simulate ballistic experiments, and although a complete description of an event through to perforation was not possible, he was able to isolate many of the important features of the penetration problem. The ceramic tile was seen to load the projectile nose causing attrition and deceleration, at a rate governed by the yield strength of the projectile material. The ceramic fractured in the form of a conoid followed by tensile failure in the ceramic initiating at the ceramic/backing plate interface, opposite the impact location. Wilkins proposed that delaying the initiation of tensile failure would substantially increase the performance of ceramic composite armours by allowing more projectile erosion.

There has been substantial interest recently in empirical studies of the failure of ceramic armour. Mayseless et al. [4] present data for targets with a range of thin backing plate materials, and also for cases where no backing is used. The backing is shown to contribute substantially to the achievement of good ballistic performance in the ceramic. Rosenberg et al. [5, 6] have used effectively semi-infinite backings and measured residual penetration depths into these as a guide to ceramic performance. They conclude that ballistic performance increases with increase in effective compressive strength of the ceramic.

Studies by Nicol et al. [7] of the energy distribution in the defeat of glass and ceramic tiles backed by thin aluminium plates, using small calibre armour piercing projectiles, demonstrated that a negligible proportion of the projectile's kinetic energy went into fracture of the ceramic. The major energy dissipating mechanisms were identified as plastic deformation of both the backing plate and the penetrator and as kinetic energy picked up by the ceramic debris and the supporting structure. The backing plates for ceramic targets were not defeated by perforation, but rather bulged and necked to failure by ductile fracture. In the case of glass tiles the projectile core was not deformed and defeated the backing plate by perforation.

While cone cracking has been studied extensively [8-12] in semi-infinite glass media, it has been studied less extensively in finite thickness bodies [13]. The ideal cone angle depends on the elastic properties of both indenter and brittle material [9], but for quasi-static ball indentations is generally around 68° to the axis of indentation. Under controlled dynamic conditions the crack travels through a time varying stress field and

hence significant, but predictable, departures from the ideal angle are observed [9]. Ballistic impact tends to be an overload situation with little control and therefore it is extremely difficult to study the sequence of cracking. Nevertheless the cone shaped zone of damage simulated by Wilkins [3] is similar to observed fracture conoids and at similar angles to cone cracks seen in quasi-static indentation of glass plates. Hornemann et al. [14] have used high speed photography to study crack propagation in the ballistic impact of glass plates. They observe not only the propagation of cracks from the impact site but also the nucleation and growth of cracks in the stress field ahead of the damage front. In the photographs of impacted glass of Pavel et al. [15] the fragmented glass debris is ejected at a similar velocity to the rate of penetration by the projectile.

The experimental and computational studies leave many gaps in our understanding of the perforation of ceramics. This work presents approximate model solutions which allow computations on ballistic impacts into ceramic composite armours, with both thick backing and thin backing, relative to the projectile calibre. The cone crack formation, ceramic and projectile erosion and backing deformation as well as the inertial response of the system components are realistically modelled. The principal observed features associated with trends in ballistic performance with changes in ceramic and backing thickness, ceramic and backing materials, projectile type and impact velocity are observed in the computational results. Predictions are generally of the correct magnitude and in many cases quite accurate. The solutions allow the mechanical principles to be studied, and can direct attention to those aspects, such as *ceramic strength properties* relevant to cracking and erosion, which need to be more closely studied.

2. APPROXIMATE NUMERICAL CONSIDERATIONS

Figure 1 shows the computer simulation of the impact of a steel penetrator on a ceramic composite target which Wilkins [3] demonstrated was close to the observations on flash radiographic images of an experimental trial. The sequence of figure 1 can be used for some approximate calculations which are instructive in guiding the modelling of such an event. From the deceleration of the projectile and its mass one can calculate the force retarding the rear of the projectile as around 100 kN which is close to the yield force of 91 kN, estimated from the projectile hardness and cross sectional area. One can conclude *reasonably therefore that the force* retarding the projectile is governed by plastic yielding of the projectile where it interacts with the ceramic, as did Wilkins [2].

In the region bounded by the cone crack, the use of a triangular velocity profile, and estimation of the mass of ceramic and metal being accelerated, gives a resultant force accelerating the target material of about 130 kN. The force acting on the target material due to impact is the yield force of the projectile (about 100 kN estimated above) plus the change in momentum according to Tate's [16] approximate theory of penetration. From the mass loss the estimated force due to a change in momentum is 53 kN, giving a total force acting on the target of 153 kN. The force resisting plate acceleration is the total force acting, 153 kN, less the resultant, 130 kN, or about 23 kN. If the ceramic is assumed to present no strength along the cracked conical boundary one can use simple plasticity calculations to estimate from the flow stress of the aluminium that the resistance offered by the backing is 100 kN if it came from shear at the periphery of the conical region or 33 kN if it came from dishing deformation. From these approximate computations it is therefore possible to state with a high degree of confidence that resistance to the penetrator is provided by inertia of the ceramic and backing bounded by the cone crack, and by dishing deformation of the backing. Using such simple calculations it is also possible to show that at the time when the projectile has decelerated and target material accelerated to a common intermediate velocity, the displacement of the back of the target is only a few

6

millimetres, in contrast to final deflections of 15 to 25 mm observed in typical perforated aluminium backing plates. The conclusion therefore is that the second stage of perforation involves the penetrator and target material bounded by the cone, moving forward resisted by bending and membrane forces in the backing till either they are slowed to zero velocity or rupture of the backing occurs. These concepts form the basis for modelling the perforation of ceramic composites with thin backing plates.

In figure 1 the simulation shows evidence of a decrease in ceramic thickness with time, erosion, and some criterion for estimating the load at which the ceramic is eroded is required. The rate of erosion will be determined by yielding and cracking beneath the penetrator. Quasi-statically a blunt indenter forced into a ceramic causes yielding and fracture and the pressure beneath the indenter is a measure of hardness of the ceramic. Continued quasi-static indentation requires a pressure equal to the material hardness. Figure 2 shows a typical Vickers indentation in an alumina tile where cracking is evident from the corners of the indent. If ceramics are assumed to obey the same laws of plastic flow as metals then the uniaxial flow stress can be obtained approximately from the hardness by dividing by 2.9 [17]. Pavel et al. [15] show the reduction in velocity of an effectively non-deforming penetrator fired through glass. The velocity reduction expected can readily be calculated assuming the force resisting the movement of the penetrator is some factor of the uniaxial yield stress of the glass, as estimated by dividing the hardness by 2.9, and taking account of the fact that approximately one calibre at the back of the glass plate is ejected with negligible resistance. Such computations are compared with the empirical data of Pavel et al. [15] in figure 3, where it appears the resisting force is reasonably taken as the uniaxial flow stress of the glass. For a metal perforated by a pointed projectile it would be twice that flow stress [18], and if the flow pressure was equal to the hardness of the ceramic then a larger deviation from experiment would be expected in this instant. An equivalent experiment for a ceramic is not available, and typical ceramic toughnesses are significantly higher than those of glass [19] indicating that chipping may be expected at a somewhat higher pressure in ceramics. The appropriate pressure at which ceramic erosion takes place is thus expected to be somewhere between the uniaxial flow stress and the hardness, but is left open for detailed comparison of computations with experiment for actual targets.

3. MODEL DEVELOPMENT

(a) Physical Concepts and Assumptions

The main features associated with perforation of a ceramic armour with a thin backing plate are shown schematically in figure 4(a). In modelling the process it was assumed that crack propagation was sufficiently fast compared to the projectile velocity that the cone crack separates the loaded region inside the cone from an unloaded region outside the cone. Based on the approximate calculations outlined previously the ceramic inside the cone and the backing plate bounded by the base of tne cone are accelerated forward with a velocity profile allowing compatibility with both the flat ended projectile and the dishing of the backing plate. As shown in figure 4(b) the more realistic velocity profile was slightly modified for computational efficacy in the model, the effect of this change being negligible as the base diameter of the cone is generally far greater than the projectile diameter. Because of the lack of knowledge on cone angle as a function of impact parameters, it was decided to use an angle between the normal to the ceramic surface and the cone side of 68° for all computations, at least consistent with quasi-static observations on simple systems.

At the front of the penetrator erosion of projectile material is taking place. In practice with brittle penetrator materials this may be in "chunks", however as the physics of such an attrition process is not developed it was assumed that projectile erosion, whether by a cracking or a shearing mechanism, was governed by plastic flow of the penetrator material. Similarly if the velocity is high enough, yielding and fracture of the front of the ceramic will be observed. This is again considered as leading to erosion of ceramic in contact with the projectile, governed by the normal load which the ceramic can sustain, whether this is estimated by indentation hardness or by uniaxial flow stress as discussed in particular cases below.

The lumped parameter model for the inertial response of the system is represented in figure 4(c). In any time step Δt a mass ΔM_P and a mass ΔM_C of projectile and ceramic respectively are eroded. M_p is the oncoming projectile mass and M_T the mass of target being accelerated. Force F_p resists forward movement of the projectile and F_T resists acceleration of the target. F_C is a measure of the strength or collapse load of the ceramic and at the interface F_I is determined by ceramic and penetrator strengths and the rate of ceramic and penetrator erosion. After some time of interaction a number of consequences can ensue, viz. The system can slow to zero velocity stopping the projectile or the projectile can be completely eroded and thus stopped. The ceramic can be eroded to zero thickness and if there is still a velocity difference between the projectile and the backing the projectile may perforate or, if there is no residual velocity difference, the backing may continue to bulge till either the velocity is reduced to zero or bursting of the bulge occurs. Without complete ceramic erosion the components may come to some constant intermediate velocity and perforation occur if the residual momentum is sufficient to continue bulging of the backing plate and cause rupture. The model for ceramic composite armours with thin backing is divided into two stages which treat target acceleration using the model of figure 4(c), followed by an examination of target failure.

(b) Target Acceleration

The equations of motion of the system in figure 4(c) are:

$$F_P = - M_P \ddot{U}_P \qquad \text{1(a)}$$

$$F_I - F_P = - \Delta M_P \dot{U}_P / \Delta t \qquad \text{1(b)}$$

$$F_C - F_I = - \Delta M_C \dot{U}_C / \Delta t \qquad \text{1(c)}$$

$$F_T - F_C = M_T \ddot{U}_T \qquad \text{1(d)}$$

where   F is force,

M is mass,

Δt is the time increment,

$\dot{U}$ and $\ddot{U}$ are velocity and acceleration respectively,

and   subscripts P, I, C and T refer to penetrator, interface, ceramic and target respectively as in figure 4(c).

8

Each of the equations (1) relates the force on an element to the change in momentum by either acceleration, U, or mass change, ΔM. The sign in equation (1b) is such that if $F_I > F_P$, ΔM_P is negative, i.e. there is a mass loss from the penetrator. The sign in equation (1c) is such that if $F_I > F_C$, $\Delta M_C \dot{U}_C$ is positive, i.e. there is an increase in momentum of the ceramic material which is moved out of the way. At the interface the approach of the penetrator and target in time step Δt is related to the loss in mass of penetrator and target. As a flat ended cylindrical penetrator of cross sectional area A_o is being treated, we can imagine a column of penetrator and ceramic being squeezed out giving continuity equations of the form:

$$\Delta M_P / \rho_P A_o = - (\dot{U}_P - \dot{U}_C) \Delta t \qquad \text{2(a)}$$

$$\Delta M_C / \rho_C A_o = (\dot{U}_C - \dot{U}_T) \Delta t \qquad \text{2(b)}$$

where ρ is the material density.

Constitutive equations for the failure of penetrator and ceramic can be established by requiring that for erosion of a column of material to occur, a value of flow stress, Y, must be exceeded, whether this is governed by uniaxial yield stress, hardness or some other measure of strength. Then for erosion to occur

$$F_P = Y_P A_o \qquad \text{3(a)}$$

$$F_C = Y_C A_o \qquad \text{3(b)}$$

In the course of solving the equations, erosion of both ceramic and penetrator did not necessarily occur; erosion requires that F_I in equation (1) exceed the relevant force F_P or F_C.

Equations (1) to (3) represent a very simplified concept of the interaction, with gross assumptions on the lumping of elements of material into composite masses. The view of ceramic compression in a simple column is expedient and the issue of failure or erosion stress level for the ceramic must be addressed. The contribution of radial inertia to projectile deceleration is ignored, as it is difficult to include in the form developed by Johnson [19], as erosion in a single front element leads to the force becoming unrealistically large as the time step, and hence the height of that front eroding element also, becomes small. Elimination of $\dot{U}_C$ and ΔM_C from the equations yields a quadratic which can be solved at each time step for the only unknown parameter, the penetrator mass loss ΔM_P. At each time step all other parameters can be updated and the solution then repeated. A relationship is required for the resistance of the target backing to bulging, F_T, and for an appropriate mass distribution to give the effective mass M_T.

Woodward et al. [20] derive an equation for the work, W, to dish a plate of thickness b and flow stress Y_T to a displacement h,

$$W = \pi b h \, Y_T \, (\frac{2}{3} b + \frac{1}{2} h) \qquad (4)$$

and it is shown that this equation gives reasonable estimates of the work done on dished backings from actual impacted ceramic composite targets, when compared with the work calculated from measurements on the plate profile. In deriving equation (4) it was assumed

the dish was in the form of a cone for calculation of stretching work, a yield moment was assumed for bending, and it was noted that the work done in tangential curvature in the conically dished region equals the work done in radial curvature (Johnson [21]). The force resisting dishing is thus obtained by differentiating equation (4) to give

$$F_T = \pi b \ Y_T \ (\frac{2}{3} b + h) \qquad (5)$$

If M_C and M_B represent masses of elements of ceramic and backing travelling at velocities $\dot{U}_C$ and $\dot{U}_B$ respectively then the total momentum of the backing is obtained by summing the momenta of individual elements. If the velocity of target material beneath the penetrator is $\dot{U}_T$, then the effective mass of the target material, M_T, can be defined by

$$M_T \dot{U}_T = \Sigma \ M_C \dot{U}_C + \Sigma \ M_B \dot{U}_B \qquad (6)$$

For the modified velocity distribution represented in figure 4(b) combined with the mass distribution of the ceramic cone and backing in figure 4(a), the effective mass becomes approximately

$$M_T = \pi D_o (\rho_C \ c/2 + \rho_B b)/12 \qquad (7)$$

where D_o is the base diameter of the cone,
               c is the ceramic tile thickness,

and other symbols and subscript notation are as used before. In cases where ceramic erosion occurred, the mass distribution was allowed to shrink in a geometrically similar manner, with the velocity dropping to zero at the new outer boundary of cone intersection with the backing. Thus D_o in equation (7) simply reduces to a new diameter proportional to the new height of the conical section. This approximation takes some account of the reduced target mass being accelerated and the reduced area of backing material which is subjected to bending and stretching loads.

(c) Target Failure

Two target failure possibilities are considered in order. For the first involving ductile instability in the backing plate, the situation after the phase of accelerating the target material is depicted in figure 5(a) with ceramic still separating the projectile from the backing plate and with projectile and backing moving forward at the same velocity. In this situation bulging of the backing plate will continue with the kinetic energy of the system being dissipated in plastic deformation of the backing, terminated by either a reduction to zero velocity or rupture as in figure 5(b). In practice the hinge in the backing plate may be expected to move radially and substantial elastic deflections occur, particularly in thin plates. These aspects are, however, not easily treated. The simplified approach used to obtain a solution considers the bulging plate as ideally plastic, with the hinge located at the cone base and uses equation (4) to calculate the work done. Perforation occurs if there is sufficient kinetic energy left in the projectile, ceramic and backing after the acceleration phase to continue plate bulging to rupture. Thus a bulge height at plate rupture is required, i.e. a failure criterion.

Backing material stress/strain properties were curve fit to an equation of the form

10

$$\bar{\sigma} = A + B\,\bar{\epsilon}^{\,n} \qquad\qquad (8)$$

where $\bar{\sigma}$ and $\bar{\epsilon}$ are effective stress and strain, and A, B and n are constant curve fitting parameters for the material. The strain at instability, ϵ_i, in a biaxial tension test can then be obtained by solving the equation

$$11B\,\epsilon_i^{\,n+1} - 4(2n + 1)B\epsilon_i^{\,n} + 11A\,\epsilon_i - 4A = 0 \qquad\qquad (9)$$

which is a variation on the form used by Johnson and Mellor [22] because of the different curve fitting relationship for stress and strain, equation (8). Equation (9) is easily solved iteratively by computer. For hydraulic bulging of circular plates the strain at instability can be related to the displacement using the assumption that the particles in the membrane describe circular paths. For the velocity profile of figure 4(b), the backing plate is going to deform into the shape of a cone. For simplicity it was assumed that the cone is uniformly tapered from the instability strain at the centre, ϵ_i, to the thickness of the original plate at the cone diameter D_o. Then if θ is the angle between the base and side of the cone, as in figure 5(b), constant volume deformation requires

$$\epsilon_i = \ell n\,(3\,\cos\,\theta - 2) \qquad\qquad (10)$$

Thus from the material characteristics, equation (8), the instability strain is calculated using equation (9), which is substituted into equation (10) to obtain the angle through which the sides of the cone are bent at failure. From simple geometry the displacement, h, of the cone is calculated and this is substituted into equation (4) to calculate the dishing work.

If ceramic erosion has occurred during the target acceleration phase then the area of the backing loaded will be reduced as discussed earlier. The assumed reduced dimensions of the cone and loaded backing after the target acceleration stage are shown schematically in figure 5(c), in relation to the initial dimensions. The velocity profile is shown in figure 5(d), where it is assumed for computational ease that the velocity drops to zero at the reduced outer hinge diameter, D_R. The reduced diameter combined with the deflection angle at failure from equation (10) leads to a lower failure displacement and hence work done in dishing failure using equation (4), than would be the case if no ceramic erosion occurred. It was assumed that only the momentum of the projectile, the ceramic and the backing material within the reduced dimensions acted to continue bulging. Thus using the simpler velocity distribution of figure 5(d) the effective kinetic energy, E_K, to equate to the work done by equation (4) is

$$E_K = \frac{1}{2}M_P\dot{U}_P^{\,2} + \frac{\pi}{8}(\rho_C c/5 + \rho_B b/3)\left(\frac{D_R^{\,2}\,\dot{U}_T}{D_R - D_P}\right)^2 \qquad\qquad (11)$$

where the ceramic thickness c is the reduced thickness after erosion, and D_P is the penetrator diameter. The effects of using reduced dimensions when accounting for the effects of erosion will be discussed in considering sample computations.

11

If the ceramic is eroded to zero thickness during target acceleration, then a projectile of higher relative velocity bears on the backing material and an alternative second failure criterion is needed. For failure it was considered the velocity at which the backing was moving did not contribute to perforation and that it was the difference in projectile/target velocity which allowed perforation. Thus the equation to determine whether the penetrator would perforate in this case was

$$\frac{1}{2} M_P (\dot{U}_B - \dot{U}_P)^2 = \pi D_P^2 b Y_T/2 \qquad (12)$$

where Y_T is the target flow stress, and subscript B represents backing. The method assumes a simple ductile hole formation mode of failure and the equation is due to Taylor [23, 18].

The set of equations described for the acceleration and failure stages was written into a computer program, CEP, which treats perforation of ceramic composite targets with thin backing plates. The program is listed in Appendix I with typical input and output. Examples of computations performed with the method are compared with experimental data below.

(b) Composites with Thick Backing

For cases with very thick backing materials it was found that the ceramic can be completely eroded with a relatively small increase in velocity of the backing. In addition the treatment of thick plate perforation with a dishing model is inappropriate. Therefore a simplified model for the first phase was developed where the interaction of the penetrator and the ceramic only are considered, with the thick backing remaining stationary. The residual penetrator, after eroding the ceramic, then interacts with the backing using a plugging model for finite thicknesses or a deep penetration model for effectively semi-infinite backings. The method also has the advantage of allowing direct checking of the ceramic erosion model against data of the type produced by Rosenberg et al. [5, 6] using semi-infinite targets.

The concept of interaction with a thick target is shown in figure 6(a) and the lumped parameter model is illustrated in figure 6(b). It is assumed that spreading of the load by the ceramic conoid is sufficient to allow negligible yielding of the backing plate. Then for a very large effective target mass M_T we obtain

$$\ddot{U}_T = \dot{U}_T = 0 \qquad (13)$$

so that the solution of equations (1) to (3) becomes trivial. There is no requirement for a resisting force of the backing (F_T). A computer program ECS was written which solves the simplified equations and is listed with typical input and output in Appendix II. In running the program, depending on the input parameters the penetrator can be stopped before the ceramic is eroded, the penetrator can be completely eroded before it perforates the ceramic, or the ceramic itself can be eroded to zero thickness. In the latter case the output lists the residual average projectile mass and velocity.

Using the output from ECS, the plugging program PLUG [24, 25] can be used to see if a thick backing is perforated by plugging by a flat ended fragment, or the program SLAM [26, 27] can be used to calculate the residual depth of penetration into a semi-infinite

12

metal target.   An alternative simpler approach is to use the equation

$$\frac{1}{2} M_P \dot{U}_P^2 \gtrless \frac{\pi}{2} D_P^2 Y_T b \qquad (14)$$

to relate the residual kinetic energy (LHS) to the work done in ductile hole formation (RHS).   Here the symbols are as used before, except that b is the thickness of a finite backing in which case the inequality determines whether penetration occurs, or for a semi infinite target b becomes the depth of penetration using the equality.   Equation (14) uses the simpler Taylor model of ductile hole formation [23, 18] and is equivalent to equation (12) for the thinner targets.   This last approach is expected to be less accurate for the blunt fragments exiting from the ceramic and was not generally used in this study, however is presented as it is a useful simpler form.   The most satisfying aspect of the models for thin and thick backings is that when the same strength, Y_C, is used for the ceramic, it is observed that thin target and thick target approaches tie together well at the transition with increasing backing thickness.   The most significant approximation, which prevents extension to very high velocities is the neglect of radial inertia which has not been included for the same reasons it has not been included in the thin backing model, i.e. a mathematically suitable treatment is not available.

4. SELECTION OF MATERIAL STRENGTH DATA

The penetrator undergoes large strain plastic flow on impact with the ceramic, thus a figure for ultimate tensile strength can be used in the modelling of its deformation.   Because in many cases penetrators impacting a ceramic are hard, they are materials where there is little work hardening and within the accuracy of the model a figure for yield stress or the approximate equivalent, Diamond Pyramid Hardness divided by 2.9 [17], should also be satisfactory.   Work hardening is not included in the model so the response of the penetrator is determined entirely by its assumed ideal rigid/plastic resistance to plastic flow.   Diamond Pyramid Hardness data is simple to obtain.

The metallic backing material has a failure strain dependent on its work hardening properties, and backing material stress strain data was therefore fitted to equation (8) for the thin target problem.   For the thick backing or semi-infinite backing problems, curve fitting of the backing material and projectile data to appropriate forms for thick target penetration models was also required [24-27].

The major decision involves the selection of a suitable strength level for the ceramic representing its resistance to the penetrator or resistance to ceramic being displaced or eroded.   Quasi-statically the resistance to indentation is given by the Diamond Pyramid Hardness, which is a stress, easily measured, figure 2, and ideal for use as a measure of ceramic strength in the model.   Alternatively it has been shown that the glass penetration data of Pavel et al [15], figure 3, is well fitted if a flow stress determined as hardness divided by 2.9 [17] is utilized.   Initial computations using some data presented by Mayseless et al. [4], figure 7, show an underestimate of the 12.7 mm Berkeley data, however the computations also showed the ceramic was not eroded under these conditions so there was no test of the appropriate flow stress properties of the ceramic.   The comparison with the 7.62 mm data of Wilkins given in the same work indicates an underestimate if hardness

divided by 2.9 is used as the ceramic flow stress and an overestimate by about the same amount if hardness is used, figure 7(a). The separation into two distinct slopes of the plots of theoretical curves for Wilkins experiments in figure 7(a), particularly noticeable for the lower strength level computations, is due to the onset of erosion at the higher backing thickness, where the impact velocity to cause perforation is necessarily higher, and the consequent shrinking of the loaded zone as depicted in figure 5(c). On the basis of this data it appears that hardness divided by some factor between 1.0 and 2.9 is an appropriate strength parameter for the ceramic. This would mean that cracking and ejection of material is easy and reduces the build-up of hydrostatic constraint in the dynamic problem.

Comparison with the full range of data provided by Wilkins [1] for four ceramic thicknesses did not, however, fit this picture exactly. To fit Wilkins data it was necessary to increase the ceramic effective strength with thickness such that for thick plates the appropriate strength is close to the hardness. The fit to Wilkins [1] data using hardness as the effective ceramic strength is shown in figure 8. It is best described as a reasonable fit to the data. Rather than curve fit exactly to empirical data by playing with strength parameters, it was decided to use hardness throughout as the strength measure and concentrate on the reliability of the computational approach and what it illustrates in the physics of perforation of ceramic composite armours.

Several other measures of strength are possible. The most obvious is the Hugoniot elastic limit, however this was not used as it is difficult and expensive to generate the data, values are tabulated for only some ceramics of interest and in any case the values are similar to the strength levels in hardness tests. The conflict of the above approach with the glass data of Pavel et al. [15] as shown in figure 3 is at this stage attributed to the very low fracture toughness of glass compared with the typical armour ceramics, which would allow glass to fragment easily producing stress relief. Ceramic and glass are then considered separate situations to be modelled.

5. COMPARISON WITH EMPIRICAL DATA

The value of the model in terms of analysing and describing the mechanisms involved in perforation of ceramic composite targets is best appreciated by comparing computations with existing experimental data. Such a process also allows the limitations of inbuilt assumptions to be tested. Comparison is made with data of several types from several sources. In all cases ceramic strength and material stress/strain data was gleaned from the best sources available, however, in general, whilst it may be for the same material type and condition as used in the experiments, it should best be described as typical.

The fit of computations to the results of Mayseless et al. [4] in figure 7(a) could be considered reasonable. For the calculations on the Berkeley experiments there was no erosion of the ceramic and variations in ceramic strength will not improve the agreement. For all these computations the projectile erosion was part of the output and this is compared with the experimental curve of Mayseless et al. [4] for projectile erosion in figure 7(b). The form is correct, however there is an underestimate of about two or three millimetres in the amount of erosion. As the model is for a flat ended penetrator, and the experimental work involved penetrators with a pointed nose several millimetres in length which would be readily broken, the difference between the experiment and the model is easily understood. In fact at very low velocities the experimental data shows a step jump in the magnitude of erosion.

The influence of ceramic erosion on predictions of the model is illustrated in the computations of figure 8. The reason for the two distinct slopes in the calculated curves is

the reduction in the effective loaded volume of ceramic and backing as represented in figure 5(c); without this change in volume the graphs would continue at the initial slope. It is noted that for each ceramic thickness the slope change in the calculated curves occurs consistently over a narrow velocity range which is determined by the ceramic strength. In contrast to this Wilkins' experimental data shows a discontinuity consistently occurring at approximately the same backing thickness for each of the ceramic thicknesses. The most plausible explanation of this difference is that a lower stiffness in thinner ceramic tiles allows easier bending to a strain at which fracture is initiated, reducing the effective strength of thinner tiles. The overall agreement between the calculations and the experiment is seen to be good when the pairs of experimental and calculated curves are examined individually. As indicated above, one can improve the fit by selecting appropriate ceramic strength figures which increase with tile thickness, however this then becomes a curve fitting exercise with less meaning in the results. Certainly a valid approach would be to use ballistic testing and the model together under conditions where ceramic erosion is expected, in order to gauge the effective ceramic strength for those impact conditions. Rosenberg and Yeshurun [6] pointed out that, contrary to their expectations, some of Wilkins' data shows no correlation between ballistic efficiency and compressive strength. From the present model this is in fact seen to be quite reasonable as Wilkins' data generally refers to conditions with backings which are thin enough that ceramic erosion, and hence strength, is of no significance. Under such conditions the effects of the ceramic are to induce erosion of the softer penetrator, and in the mass of ceramic cone material which must be accelerated. The experiments of Rosenberg and Yeshurun [6] are on semi-infinite backings. As seen in figure 8, even for the relatively low strength AD-85 alumina, it is with the thicker backing where erosion of the ceramic occurs that the ceramic strength limits the rate of increase in performance with backing thickness.

The effect of ceramic and backing thicknesses are again shown in figure 9 for the data of Wilkins et al. [2] using aluminium backed boron carbide tiles. The calculations give the correct ordering with ceramic and backing thickness and are as close to the experimental data as could be expected given the approximations in the model. In this case the model predicts no ceramic yielding, and hence no erosion, of the tiles. This is not meant to imply that the ceramic does not fragment, just that in the time frame of the ballistic event it is not eroded from its position ahead of the projectile. That ceramic fragmentation and erosion are not necessarily the same is shown by figure 10 which shows debris from the impact of an armour piercing round on an AD85 alumina target. Despite significant fragmentation the result of inertia and a resilient adhesive bond is to keep a large part of the fracture conoid in place.

Results for three different ceramics are shown in figure 11. The slight differences predicted by the model result from density differences which determine the mass of ceramic to be accelerated, and by the yielding of the AD85 alumina leading to a slope change at the highest velocities. The predictions of ballistic limits are extremely good. On this scale the model orders the ceramics incorrectly compared with the experiments, however if areal density was used rather than tile thickness to plot the data, the experimental and model results would separate into three distinct sets in the correct order, because of large density differences between the three materials, i.e. on the thickness scale that Wilkins et al. [2] used to plot the data the model is not sensitive to the differences.

The formulation of the present model uses stress/strain behaviour suitable for a metallic backing, hence some composite materials are presently excluded from consideration. However, Mayseless et al. [4] show data for a range of backing materials including several metals allowing the effect of backing material to be examined for some cases as in figure 12. This comparison shows the calculated magnitude and ordering of performance using the model to be correct, however for these results the model consistently underestimates the ballistic limits.

Wilkins [1] also presented a comparison of the performance of sharp and blunt penetrators against AD85 alumina. The present model is for blunt penetrators and its ballistic limit predictions are compared with Wilkins' [1] data in figure 13. Unfortunately the computations fit the sharp penetrator data better. This comparison, whilst emphasising the effect of nose shape, highlights the approximate nature of the present approach.

The model treatment for the situation of a thick backing can be compared with data of Bless et al. [28] who backed alumina tiles with semi-infinite aluminium blocks. The experimental data comprise the depth of penetration into a semi-infinite block, X, compared with the depth when the block is covered with a ceramic tile, R, as presented in Table 1, where the ceramic tile thickness is C. Computations of penetration into the semi-infinite block were made with a deep penetration model [26, 27] using the initial impact conditions to calculate X. For the case with the ceramic tile the program ECS was used to treat the ceramic penetration and the output from these calculations used as input for the same deep penetration model to calculate R. In a small number of cases in which a sharp, hard penetrator was involved, a ductile hole formation model was more appropriately used for the calculations into a semi-infinite aluminium block. In the majority of cases Table 1 shows reasonable agreement. In most of those where agreement is poor, the impact velocity was far in excess of that where any of the models are expected to work (i.e. > 1.5 km s^{-1}). In a couple of cases where computational agreement was obtained, where the impact velocity was beyond the range of the models, it is considered a coincidence in the present instance, and these cases are not highlighted in Table 1 as effective computations. At least in one case (Shot 4-452) Bless et al. [28] indicate that their "experimental" depth of penetration is only "estimated".

In making the above calculations with the program ECS for the thick backing problem it was noted that ceramic erosion occurred whilst the penetrator was above some critical velocity depending on the ceramic strength. Below this velocity only the penetrator was eroded and decelerated with the calculations stopping when the penetrator was reduced to zero mass or velocity. In those cases where the impact velocity was just above the value for erosion of the ceramic, the deceleration during the interaction was sufficient to reduce the projectile velocity below the critical value and ceramic erosion stopped before the ceramic in front of the projectile was completely removed. In all cases where the ceramic was not perforated Table 1 shows zero residual perforation. In practice a few millimetres of deformation is always observed due to fracture of the ceramic and impact of the residual debris.

The effectiveness of the deep penetration model for doing the part of the calculation involving penetration into the metal backing was checked using comparisons with the calibration data of Bless et al. [28] in figures 14(a) and 14(b) for tantalum rods and fragment simulating projectiles respectively. The comparisons of Table 1 and Fig. 14 indicate that the approach used to treat targets with thick backings may give good estimates of behaviour up to impact velocities of the order of 1.5 km s^{-1}.

A final comparison is with data of Rosenberg and Yeshurun [5, 6] who define a ballistic efficiency (η) of a ceramic as

$$\eta = \frac{\rho_{Al} P^*_{Al}}{\rho_c h^*_c} \tag{15}$$

where $\qquad$ h^*_c is the minimum ceramic thickness required to prevent penetration into a thick aluminium backing,

P^*_{Al} is the penetration depth of the projectile into bare aluminium, and

ρ_{Al} and ρ_{c} are the densities of aluminium and ceramic respectively.

The ballistic efficiency is then obtained from the slope of a graph of $\rho_{Al}h_{Al}$ versus $\rho_{c}h_{c}$ and the results of Rosenberg and Yeshurun [5, 6] are represented as a continuous straight line in figure 15 for AD85 alumina.

The points of intercept on the ordinate and abscissa for defining the line of slope η may be found from the model solutions using the following procedure. As the penetrator is sharp and hard the depth of penetration into a semi-infinite target is estimated using the ductile hole formation model [18, 23], and as figure 15 shows this point is where the Rosenberg and Yeshurun line for AD85 meets the ordinate. The ceramic penetration model for the thick backing case, program ECS, is then combined with the deep penetration model [26, 27] to calculate a curve for increasing ceramic thicknesses and thus at a range of $\rho_{c}h_{c}$ values, till the curve crosses the abscissa. The crossing points on the ordinate and abscissa are joined with a straight line to obtain the line equivalent to that of Rosenberg and Yeshurun [5, 6]. This is shown as a dashed line in figure 15 for an assumed AD85 alumina strength of 5.6 GPa. This is smaller than the 8.8 GPa used in earlier calculations because under the impact conditions of velocity, penetrator and ceramic strengths, the higher value of ceramic strength would not have allowed any penetration with the present model. A lower value of strength was therefore chosen which allowed some level of agreement to be achieved.

It is immediately noticed in figure 15 that the blunt penetrator model gives much lower penetration depth than the ductile hole formation model, where no ceramic tile is present, and this accounts for a large part of the apparent effectiveness of the ceramic. In fact the graphs indicate the prime influence of the ceramic is in destroying the projectile point, reducing substantially its penetrating capability, and represented by the discrepancy of the ductile hole formation and deep penetration models on the ordinate. It is also noted that the calculations with ceramic tiles indicate that experimental data points should only fall on a straight line of slope η by coincidence if the data is determined for thick ceramic tiles giving low values of $\rho_{Al}h_{Al}$; in fact this is where the experimental data of Rosenberg and Yeshurun [5, 6] is clustered. Finally for some of the harder ceramics tested by Rosenberg and Yeshurun [5, 6], a 12.7 mm steel cored projectile at the velocities of their experiments would not cause ceramic erosion, hence preventing impact on the aluminium backing according to the present model. In practice the experimental arrangement used without any side constraint allows easy fragmentation and ejection failure of the tile and hence easier perforation by projectile fragments. This phenomenon would not occur in a properly restrained armour configuration. At this stage therefore it is still questionable whether a ceramic strength parameter suitable for one configuration is necessarily also suitable for all other ceramic armour configurations. The three effects presented here, destruction of the projectile nose profile, real ceramic erosion effects, and unrestrained fragmentation and ejection of the tile are not linearly related to ceramic thickness. Thus the experimental method of determining the ballistic efficiency, η, may be treated as a useful technique for comparing performance, with caution in attributing a single physical meaning to the results. This comparison also raises the question of how to treat ceramic attrition, accounting for both the erosion effects at high velocity and the fragmentation at low velocity, in a model of the present form.

6. DISCUSSION

There is no pretence that the models presented in the present work are to be considered an exact simulation of the physics of impact, however the straightforward descriptions of the physics which they embody leads to reliable and relatively simple algorithms which give reasonable quantitative estimates of ceramic performance. In addition the predictions of changes with variations in ceramic and backing material type and thickness, and projectile material and dimensions are such that the models should be useful for parametric studies and for guiding experiments and design. The concepts as presented in figures 4, 5 and 6 therefore probably embody most of the principal features of the impact event. More accurate physical modelling with increased complexity of the algorithms can be expected to lead to better predictions of performance. Approximations on aspects of both the physics and the material properties are so gross that the degree of concurrence with experiment over such a wide range could be considered truly remarkable.

A major omission is the neglect of radial inertia. Not only is the momentum of eroded projectile material destroyed, but also it must be ejected laterally at some velocity. The treatment used by Johnson [19] for high rate compression was not easily adopted in the present instance as the radial inertia force becomes excessive as the thickness of the deforming zone becomes small which, with the present model, is dependent on the time step. The most profitable approach would appear to be to consider the eroded projectile material as having a momentum change associated with a velocity change from $\dot{U}_P$ to some radial ejection velocity $\dot{U}_R$, rather than by having its momentum destroyed as in the conventional modified Bernoulli approach [16]. At present the extra variable would seem to make the equations insoluble. This would however maintain the same logic as considering an increase in momentum associated with the velocity $\dot{U}_C$ picked up by the eroded ceramic, and it may be possible to relate $\dot{U}_C$ and $\dot{U}_R$ in some way.

In treating the backing deformation which is largely a dishing or bulge formation problem, the location of the hinge is a convenient conjecture. There is no doubt that in practice both significant elastic contributions to deflection and expansion of the hinge radially influence both the energy absorption and the effective observed ductility of the backing material. The simple linear thickness variation and the choice of instability criterion fortunately give overall deflections which are in accord with experience.

The deflection of the backing makes easier the radial and circumferential cracking in the ceramic. When bending occurs the resultant lack of support due to the bending allows ejection of fragmented ceramic from the back, and in addition ejection of ceramic on the impact side is resisted less than the extrusion of material when the penetrator gets deeper into the ceramic tile. For this problem there is almost a complete lack of knowledge on material continuity and consolidation at any time. The whole question of how ceramic fragmentation influences effective strength is unresolved. The use of hardness in the present instance as a guide to strength is seen to be an effective starting point.

Projectile shape is limited to the assumption of a flat ended cylinder. This is seen to highlight how approximate the model is in Fig. 13 as the model does not have the sensitivity to at least plot nearer to experimental data for the blunt projectiles. That ceramics quickly negate, by fracture, the influence of a sharp nose is highlighted by the discussion of figure 15. Questions on projectile shape will not be resolved by one dimensional models such as these and must rely on experiment and two and three dimensional simulations for detailed examination.

Despite the above difficulties, and the questions of ceramic effective strength in particular, the comparisons in this study show the models and associated computer programs, CEP and ECS, to be effective tools for the study of ceramic armour behaviour.

18

The programs should not be used for the prediction of performance, rather as a guide in understanding the interactions. Thus the program for thick backings, ECS, may, by simulating experiments, enable studies of the effective pressure at which erosion occurs and how this is influenced by material and confinement.

7. CONCLUSIONS

This work has presented two models for the perforation of ceramic composite armours, one for the perforation of targets with thin backing plates, which deform by bending away under the influence of the ceramic fracture conoid to fail by a biaxial tensile fracture, and the other for targets with a thick backing, where the backing remains undeformed whilst the ceramic erodes and is then perforated by the residual projectile fragment. The details of ceramic fragmentation are avoided in the model which treats the dynamics of movement of blocks of material with macroscopic failure criteria for both ceramic and backing. Comparisons of computations with empirical data demonstrate a good correlation, and the model can be used for parametric studies, to assist with the analysis of experimental data and for design. Ceramic hardness is used as a strength parameter, however the consideration of ceramic strength appropriate to ballistic impact is considered a major aspect for further investigation.

8. REFERENCES

1. Wilkins, M.L. (1978). Mechanics of penetration and perforation. International Journal of Engineering Science, 16, 793-807.

2. Wilkins, M.L., Cline, C.F. and Honodel, C.A. (1969). Fourth progress report of light armour program (Report UCRL-50694). Livermore: Lawrence Radiation Laboratory, University of California.

3. Wilkins, M.L. (1980). Computer simulation of penetration phenomenon. In R.C. Laible (Ed) Ballistic materials and penetration mechanics, Elsevier Sci. Pub. Co., 225-252.

4. Mayseless, M., Goldsmith, W., Virostek, S.P. and Finnegan, S.A. (1987). Impact on ceramic targets. Journal of Applied Mechanics, 54, 373-378.

5. Rosenberg, Z. and Yeshurun, Y. (1987). An empirical relation between the ballistic efficiency of ceramic tiles and their effective compressive strength. Proceedings 10th International Symposium on Ballistics, ADPA, San Diego, California.

6. Rosenberg, Z. and Yeshurun, Y. (1988). The relation between ballistic efficiency and compressive strength of ceramic tiles. International Journal of Impact Engineering, 7, 357-362.

7. Nicol, B., Pattie, S.D., O'Donnell, R.G. and Woodward, R.L. (1988). Fracture of ceramics in composite armours. In Fracture Mechanics in Engineering Practice, Conference of Australian Fracture Group, Melbourne University.

8. Frank, F.C. and Lawn, B.R. (1967). On the theory of hertzian fracture. Proceedings of the Royal Society, A299, 291-306.

9. Knight, C.G., Swain, M.V. and Chaudhri, M.M. (1977). Impact of small steel spheres on glass surfaces. Journal of Materials Science, 12, 1573-1585.

10. Lawn, B.R. and Swain, M.V. (1975). Microfracture beneath point indentations in brittle solids. Journal of Materials Science, 10, 113-122.

11. Lawn, B. and Wilshaw, R. (1975). Review indentation fracture: Principles and applications. Journal of Materials Science, 10, 1049-1081.

12. Ostojic, P. and McPherson, R. (1987). A review of indentation fracture theory: Its development, principles and limitations. International Journal of Fracture, 33, 297-312.

13. Woodward, R.L. (1988). Some aspects of cone crack propagation in finite thickness glass plates. In The Material Wealth of the Nation, Proceedings of Institute of Metals and Materials Australasia Bicentennial Conference, Sydney, Australia, 1, 111-118.

14. Hornemann, U., Rothenhausler, H., Senf, H., Kalthoff, J.F. and Winkler, S. (1984). Experimental investigation of wave and fracture propagation in glass slabs loaded by steel cylinders at high impact velocities. In J. Harding (Ed.) Mechanical Properties at High Rates of Strain, Institute of Physics Conference Series No. 70, Institute of Physics, Bristol & London, 291-298.

15. Pavel, W., Raatschen, H.-J., Schwarz, R., Senf, H. and Rothenhausler, H. (1987). Experimental and numerical investigations of the failure behavior of glass targets under impact loading by rigid projectiles. Proceedings of 10th International Symposium on Ballistics, ADPA, San Diego, California.

16. Tate, A. (1967). A theory for the deceleration of long rods after impact. Journal of the Mechanical and Physics of Solids, 15, 387-399.

17. Tabor, D. (1951). The hardness of metals. Oxford: Clarendon Press.

18. Woodward, R.L. (1978). The penetration of metal targets by conical projectiles. International Journal of Mechanical Science, 20, 349-459.

19. Johnson, W. (1972). Impact strength of materials. p 152, Arnold.

20. Woodward, R.L., O'Donnell, R.G., Baxter, B.J., Nicol, B. and Pattie, S.D. (1989). Energy absorption in the failure of ceramic composite armours. To be published in Materials Forum.

21. Johnson, W. Ibid. p. 194.

22. Johnson, W. and Mellor, P.B. (1962). Plasticity for mechanical engineers. Von Nostrand, p 187.

23. Taylor, G.I. (1948). The formation and enlargement of a circular hole in a thin plastic sheet. Quarterly Journal of Mechanical and Applied Mathematics, 1, 103-124.

24. Woodward, R.L. and de Morton, M.E. (1976). Penetration of targets by flat-ended projectiles. International Journal of Mechanical Science, 18, 119-127.

25. Woodward, R.L. and Crouch, I.G. (1988). Analysis of the perforation of monolithic and simple laminate aluminium targets as a test of analytical deformation models (MRL Report MRL-R-1111). Maribyrnong, Vic.: Materials Research Laboratory.

26. Woodward, R.L. (1982). Penetration of semi-infinite metal targets by deforming projectiles. International Journal of Mechanical Science, 24, 73-87.

27. Woodward, R.L. (1981). Modelling penetration by slender high kinetic energy projectiles (MRL Report MRL-R-811). Maribyrnong, Vic.: Materials Research Laboratory.

28. Bless, S.J., Rosenberg, Z. and Yoon, B. (1987). Hypervelocity penetration of ceramics. International Journal of Impact Engineering, 5, 165-171.

Table 1 Comparison of Calculated Penetration Depths into Aluminium Compared to Experiments of Bless et al. [15][†]

S.N.[*]	U_{o} (km s^{-1})	C (mm)	Projectile	X (mm) Exp.	X (mm) Calculation	R (mm) Exp.	R (mm) Calculation
4-324	2.55 ‖	9.3	8 g Ta rod	93	77	96	65
4-325	1.96 ‖	9.3	8 g Ta rod	74	56	84	46
6-777	1.35	9.3	8 g Ta rod	48	36	36	33
6-778	0.61	6.3	8 g Ta rod	11	9	4.8	0
6-967	0.70	9.19	8 g Ta rod, Sharp	16	12.7	5.3	0
6-958	1.66	12.7	12.7 FSP	33	27	14.8	18
6-969	1.01	9.14	12.7 FSP	17.5	14	4.8	0
4-452	2.30 ‖	9.14	7.62 APM2	91	45 (429)	64	41
9-843	0.84	9.14	7.62 APM2	48	10.8 (57)	1	0
10-452	0.78	6.35	7.62 APM2	48	8.6 (49)	1	0
9-1117	0.94	9.14	7.62 APM2	51	11.9 (72)	1	0
6-832	0.88	9.14	7.62 W2 APM2	115	19 (126)	4	11.5
6-966	1.64	9.14	7.62 APM2	73	29 (218)	30	24
4-579	2.70 ‖	9.14	6061-T6 APM2	51.5	57.5	31.3	56
4-596	2.80 ‖	9.14	7075-T6 APM2	53	61	39.4	60
6-1122	1.47	9.14	7075-T6 APM2	31	17	3	0

[*] S.N. = Shot No, U_{o} = impact velocity, C = ceramic thickness,
X = depth into aluminium with no ceramic cover,
R = depth into aluminium with ceramic tile,
FSP = Fragment Simulating Projectile.

[†] Calculations of penetration depth were generally performed with a deep penetration model [26, 27] except for cases indicated by ( ) because a hard sharp penetrator is concerned and in these cases the model of Taylor for ductile hole formation was used, i.e. equation (14). Those results which are underlined are considered effective calculations. Some reasons for poor agreement in other cases are discussed in the text. Shots No. 4-324 and 4-325 involved the use of a cover plate over the ceramic, and this was accounted for approximately in the computations.

‖ Shots thus indicated were at impact velocities far above that at which any of the models are expected to be valid.

APPENDIX 1

CEP – COMPUTER PROGRAM FOR THIN BACKING CERAMIC COMPOSITE TARGETS

The computer program CEP solves the problem of perforation of targets consisting of a ceramic tile backed by a thin ductile metal backing material. The program calls on an input file CIP.DAT and it increments projectile velocity from the initial value until a condition is found at which the ceramic is just perforated. At this velocity the program stops and creates an output file, COP.DAT, containing a number of the more useful calculated parameters. A typical input is listed at Table A1.1 and a typical output at Table A1.2, followed by a listing of the program.

Table A1.1   Typical Input CIP.DAT

Parameter	Symbol in Program	Units	Typical Value
Initial Velocity Estimate	VPO	ms^{-1}	400.
Penetrator Yield Strength	YP	MPa	2300.
Penetrator Density	ROP	$g\,cm^{-3}$	7.85
Penetrator Mass	ASP	g	30.
Penetrator Diameter	DP	mm	12.7
Penetrator Height	HP	mm	30.17
Ceramic Thickness	TG	mm	6.35
Ceramic Density	ROC	$g\,cm^{-3}$	3.4
Ceramic Vickers Hardness	HARC	GPa	8.8
Backing Thickness	TB	mm	14.
Backing Density	ROB	$g\,cm^{-3}$	2.7
Backing Strength, A eq.(8)	AB	MPa	280.
Backing Strength, B eq.(8)	BB	MPa	268.
Backing Work Hardening Exponent, n eq.(8)	ENB	–	.513

Table A1.2   Typical Output COP.DAT

RKE	WKS	WKB	TOTKE	RW	RET
651.3	717.8	165.6	1371.4	1365.2	–6.2

DIKE	CWD	VPO
0.	1669.	565.

CONE ANGLE	R	RC	TCN
22.000	0.0221	0.0221	0.006350

VPN	VTN	PH	RASP
237.6	237.6	0.02321	0.023075

STN	TI	PHID	DISP	DIST	TIME
0.514498	0.008369	30.01	0.00908	0.00431	.000027781

SYMBOL	PARAMETER
RKE	Residual kinetic energy of penetrator at end of Stage I.
WKS	Work done in stretching backing Stage I.
WKB	Work done in bending backing Stage I.
TOTKE	Target plus projectile residual kinetic energy at end of Stage I.
RW	Residual work to fail by dishing in Stage II.
RET	RW – TOTKE, if–ve dishing failure
DIKE	Difference in KE represented by differential projectile/target velocities at end of Stage I.
CWD	Work done for backing to fail by perforation.
VPO	Velocity of projectile to just defeat target.
CONE ANGLE	Fracture conoid angle in ceramic.
R	Radius of dishing region defined by original conoid.
RC	Reduced dishing radius if ceramic erosion has occurred.
TCN	Ceramic thickness.
VPN	Velocity of Penetrator at start of Stage II.
VTN	Velocity of target elements at start of Stage II.
PH	Penetrator height.
RASP	Penetrator mass.
STN	Target failure strain by biaxial instability.
TI	Target thickness at instability.
PHID	Angle of dishing in degrees.
DISP	Dishing displacement for failure.
DIST	Actual final dishing displacement at end of Stage I.
TIME	Time for Stage I, stage.

```
C      CEP.FOR
C      PROGRAM TO CALCULATE BALLISTIC LIMIT AND ENERGY CONSUMPTION
C      IN SMALL CALIBRE AP DEFEAT OF CERAMIC FACED COMPOSITES
C      WRITTEN BY RAYMOND L WOODWARD,MATERIALS RESEARCH
C      LABORATORY,MARIBYRNONG,1989
C
       OPEN(UNIT=1,FILE='CIP.DAT',STATUS='OLD')
       OPEN(UNIT=2,FILE='COP.DAT',STATUS='NEW')
   21  FORMAT(F8.1/F8.1/F10.4/F10.4/F10.4/F10.3/F10.4/
      1F8.3/F6.2/F10.3/F8.4/F10.1/F10.1/F8.3)
   41  FORMAT(T11,'RKE'T24,'WKS'T38,'WKB'T48,'TOTKE'T65,'RW'T75,'RET')
   42  FORMAT(4X,F10.1,4X,F10.1,4X,F10.1,2X,F10.1,4X,F8.1,4X,F6.1)
   43  FORMAT(4X,F10.0,4X,F10.0,4X,F10.0)
   44  FORMAT(T10,'DIKE'T25,'CWD'T38,'VPO')
   45  FORMAT(T5,'CONE ANGLE'T23,'R'T35,'RC'T47,'TCN')
   46  FORMAT(8X,F6.3,4X,F8.4,4X,F8.4,4X,F8.6)
   47  FORMAT(T8,'VPN'T18,'VTN'T30,'PH'T42,'RASP')
   48  FORMAT(4X,F8.1,2X,F8.1,4X,F8.5,4X,F10.6)
   49  FORMAT(T6,'STN'T16'TI'T24,'PHID'T36,'DISP'T50,'DIST'T63,'TIME')
   50  FORMAT(2X,F8.6,2X,F8.6,2X,F6.2,6X,F8.5,6X,F8.5,4X,F10.9)
       READ(1,21)VPO,YP,ROP,ASP,DP,HP,TC,ROC,HARC,TB,ROB,AB,BB,ENB
       YP=YP*1000000.
       ROP=ROP*1000.
       ASPO=ASP*.001
       DP=DP*.001
       HPO=HP*.001
       TC=TC*.001
       ROC=ROC*1000.
       HARC=HARC*1000000000.
       FC=.7854*HARC*(DP**2)
       TB=TB*.001
       ROB=ROB*1000.
       AB=AB*1000000.
       BB=BB*1000000.
       ASF=ASP/HP
       DT=.00000001
C
```

```
C       CALCULATE BACKING INSTABILITY STRAIN
C
        STN0=0.359
        FN0=11*BB*(STN0**(ENB+1))-(8*ENB+4)*BB*(STN0**ENB)
       1+(11*AB*STN0)-4*AB
        DO 33 N=1,10000
        STN1=STN0+.001
        FN1=11*BB*(STN1**(ENB+1))-(8*ENB+4)*BB*(STN1**ENB)
       2+(11*AB*STN1)-4*AB
        IF(FN1.EQ.0)GO TO 31
        SGN=FN1/FN0
        IF(SGN.LT.0)GO TO 30
        STN0=STN1
        FN0=FN1
   33   CONTINUE
   30   STN=(STN0+STN1)*0.5
        GO TO 32
   31   STN=STN1
   32   CONTINUE
C
C       BEGIN STEPPING VELOCITY,TILL V50 FOUND
C
        DO 101 K=1,500
        VP=VPO
        VPO=VPO+5.
        T=0
        PKE=0.5*ASP*(VP**2)
        TCN=TC
        HP=HPO
        ASP=ASPO
C
C       CONE ANGLE/RADIUS OF DISHED REGION/MASS CONE/CONSTANTS
C
        CA=.383972
        CAD=CA*57.296
        R=(TC/TAN(CA))+(DP/2)
        ASCB=3.14159*((TC*ROC/2)+(TB*ROB))*(R**2)/3
        F1=YP*0.7854*(DP**2)
```

```
      FCF=DT*(FC-F1)
      F2=F1+(VP**2)*ASF
C
C     THICKNESS AT INSTABILITY/BEND ANGLE
C
      TI=TB/EXP(STN)
      PHI=ACOS(.66666667+TI/(3*TB))
      PHID=PHI*57.296
      DISPO=(R-DP/2)*TAN(PHI)
      YSB=AB+BB*(STN**ENB)/(ENB+1)
      C1=ROC/ROP
      A=-C1/(ASF*DT)
      C3=ASF*DT*C1
C
C     TARGET ACCELERATION/PROJ. EROSION AND DECELERATION
C
      DIST=0
      VT=0
      F3=2.0944*YSB*(TB**2)
      DO72 I=1,50000
      DISP=DISPO
      T=T+DT
      DVP=F1*DT/ASP
      IF(F2.GT.FC)GO TO 14
      DVT=(F2-F3)*DT/ASCB
      GO TO 15
14    DVT=(FC-F3)*DT/ASCB
15    VPN=VP-DVP
      VTN=VT+DVT
      DIST=DIST+(VTN+VT)*DT/2
      IF(F2.LT.FC)GO TO 18
      B=-(1+2*C1)*(VP+VPN)/2+(VT+VTN)*C1/2
      C=-C3*(VP-VT+VPN-VTN)*(VP+VPN)/4-FCF
      DAS=-B/(2*A)-(SQRT(B**2-4*A*C))/(2*A)
      GO TO 19
18    DAS=-(VPN+VP-VT-VTN)*DT*ASF/2
19    DTC=((VPN+VP)*DT/2)+DAS/ASF-(VT+VTN)*DT/2
      TCN=TCN-DTC
```

```
          RC=(TCN/TAN(CA))+DP/2
          ASCB=1.0473*((TCN*ROC/2)+(TB*ROB))*(RC**2)
          DISP=(RC-DP/2)*TAN(PHI)
   91     ASP=ASP+DAS
          F3=(2.0944*(TB**2)+3.14159*TB*DIST)*YSB
          F2=F1-DAS*VPN/DT
          IF(TCN.LE.0)GO TO 88
          IF(DIST.GE.DISP)GO TO 88
          IF(VTN.GE.VPN)GO TO 88
          VP=VPN
          VT=VTN
   72     CONTINUE
   88     CONTINUE
C
C         CALC. OF ENERGIES AND OUTPUT
C
   54     PH=ASP/ASF
          DIKE=0.5*ASP*((VPN-VTN)**2)
          CWD=1.5708*(DP**2)*TB*(AB+BB*(STN**ENB))
          RKE=0.5*ASP*(VPN**2)
          WKS=2.0944*(TB**2)*DIST*YSB
          WKB=1.5707*TB*(DIST**2)*YSB
          TKE=3.14159*(RC**4)*(VTN**2)*((TCN*ROC/20)+(TB*ROB/12))
          1/((RC-DP/2)**2)
          TOTKE=RKE+TKE
          RW=3.14159*TB*YSB*(.6667*TB*(DISP-DIST)+0.5*((DISP**2)
          1-(DIST**2)))
          RET=RW-TOTKE
C         FAILURE BY DISHING IN STAGE 2
          IF(RET.LT.0)GO TO 102
C         FAILURE BY PERFORATION
          IF(DIKE.GT.CWD)GO TO 102
C         FAILURE BY DISHING IN STAGE 1
          IF(DIST.GE.DISP)GO T ` 102
  101     CONTINUE
  102     WRITE(2,41)
          WRITE(2,42)RKE,WKS,WKB,TOTKE,RW,RET
          WRITE(2,44)
```

```
WRITE(2,43)DIKE,CWD,VPO
WRITE(2,45)
WRITE(2,46)CAD,R,RC,TCN
WRITE(2,47)
WRITE(2,48)VPN,VTN,PH,ASP
WRITE(2,49)
WRITE(2,50)STN,TI,PHID,DISP,DIST,T
STOP
END
```

ECS – PROGRAM FOR CERAMIC PERFORATION WHEN BACKED BY A THICK PLATE

The computer program ECS solves the problem of perforation of a ceramic tile when it is supported by a very thick backing which shows negligible deflection until the ceramic block is completely eroded. The program calls on the input file EIS.DAT and produces an output file EOS.DAT showing residual projectile mass and velocity after ceramic erosion. The latter data can then be fed into an appropriate model to examine the perforation of the backing. A typical input is listed at Table A2.1 and the corresponding typical output at Table A2.2, followed by a listing of the program.

Table A2.1   Typical Input EIS.DAT

Parameter	Symbol in Program	Units	Typical Value
Penetrator Velocity	VP	ms^{-1}	1200.
Penetrator Yield Stress	YP	MPa	2500.
Penetrator Density	ROP	$g\,cm^{-3}$	7.85
Penetrator Mass	ASP	g	23.1
Penetrator Diameter	DP	mm	10.8
Ceramic Thickness	TC	mm	6.
Ceramic Density	ROC	$g\,cm^{-3}$	3.4
Ceramic Vickers Hardness	HARC	GPa	8.8

Table A2.2   Typical Output EOS.DAT

TCN	VPN	ASP	T
0.00555	1190.0	0.02256	0.00000100
0.00511	1179.7	0.02203	0.00000200
0.00469	1169.2	0.02149	0.00000300
0.00428	1158.4	0.02095	0.00000400
0.00388	1147.3	0.02040	0.00000500
0.00350	1135.9	0.01986	0.00000600
0.00313	1124.2	0.01931	0.00000700
0.00278	1112.2	0.01876	0.00000800
0.00244	1099.8	0.01821	0.00000900
0.00212	1087.0	0.01765	0.00001000
0.00182	1073.9	0.01709	0.00001100
0.00154	1060.2	0.01652	0.00001200
0.00127	1046.1	0.01596	0.00001300
0.00103	1031.5	0.01538	0.00001400
0.00081	1016.3	0.01480	0.00001500
0.00062	1000.6	0.01422	0.00001600
0.00044	984.1	0.01363	0.00001700
0.00030	966.9	0.01303	0.00001800
0.00019	948.9	0.01242	0.00001900
0.00010	930.0	0.01181	0.00002000
0.00006	910.1	0.01118	0.00002100
0.00005	889.0	0.01054	0.00002200
0.00005	866.6	0.00991	0.00002300
0.00005	842.8	0.00929	0.00002400
0.00005	817.3	0.00870	0.00002500
0.00005	790.0	0.00812	0.00002600
0.00005	760.8	0.00756	0.00002700
0.00005	729.4	0.00702	0.00002800
0.00005	695.5	0.00651	0.00002900
0.00005	659.0	0.00602	0.00003000
0.00005	619.4	0.00556	0.00003100
0.00005	576.6	0.00513	0.00003200
0.00005	530.2	0.00474	0.00003300
0.00005	479.8	0.00437	0.00003400
0.00005	425.4	0.00405	0.00003500
0.00005	366.6	0.00376	0.00003600
0.00005	303.7	0.00352	0.00003700
0.00005	236.7	0.00333	0.00003800
0.00005	166.2	0.00318	0.00003900
0.00005	93.0	0.00309	0.00004000
0.00005	18.3	0.00305	0.00004100
TCN	VPN	ASP	T
0.00005	–0.5	0.00305	0.00004125

| Symbol	Parameter
TCN	Ceramic Thickness (m)
VPN	Penetrator Velocity (ms^{-1})
ASP	Penetrator Mass (kg)
T	Time (S)

In each case the value under the symbol is the final value.   In the above example ceramic erosion had stopped after 2 microseconds because the penetrator velocity was reduced below the value at which the ceramic strength was exceeded.   Projectile erosion continued till the penetrator velocity was reduced to zero after 42.5 microseconds.

```
C       ECS
C       PROGRAM FOR CALCULATING CERAMIC/PROJ. EROSION WHEN BONDED
C       TO A SEMI-INFINITE PLATE
C       WRITTEN BY RAYMOND L WOODWARD,MATERIALS RESEARCH
C       LABORATORY,MARIBYRNONG,1989
        OPEN(UNIT=1,FILE='EIS.DAT',STATUS='OLD')
        OPEN(UNIT=2,FILE='EOS.DAT',STATUS='NEW')
21      FORMAT(F8.1/F8.1/F10.4/F10.4/F10.4/F10.4/F8.3/F6.2)
47      FORMAT(T8,'TCN'T18,'VPN'T30,'ASP'T42,'T')
48      FORMAT(4X,F8.5,2X,F8.1,4X,F9.5,4X,F10.8)
        READ(1,21)VP,YP,ROP,ASP,DP,TC,ROC,HARC
        YP=YP*1000000.
        ROP=ROP*1000.
        ASP=ASP*.001
        DP=DP*.001
        TC=TC*.001
        TCN=TC
        ROC=ROC*1000.
        HARC=HARC*1000000000.
        YC=HARC/1.0
        ASF=.7854*ROP*(DP**2)
        F1=YP*.7854*(DP**2)
        T=0
        DT=.00000001
        F3=YC*.7854*(DP**2)
        FCF=DT*(F3-F1)
        C1=ROC/ROP
        A=0-C1/(ASF*DT)
        C3=ASF*DT*C1
        F2=F1+(VP**2)*ASF
        DO 72 I=1,50000
        T=T+DT
        DVP=F1*DT/ASP
        VPN=VP-DVP
        IF(F2.LT.F3)GO TO 18
        B=0-(VPN+VP)*(1+2*C1)/2
        C=0-C3*((VPN+VP)**2)/4-FCF
        DAS=0-B/(2*A)-(SQRT(B**2-4*A*C))/(2*A)
        GO TO 19
18      DAS=-ASF*(VPN+VP)*DT/2
19      DTC=((VPN+VP)*DT/2)+DAS/ASF
        TCN=TCN-DTC
        ASP=ASP+DAS
        VP=VPN
        F2=F1-DAS*VPN/DT
        DO 83 N=1,500
        INC=N*100
        IF(I-INC)84,79,83
83      CONTINUE
79      WRITE(2,48)TCN,VPN,ASP,T
84      IF(ASP.LE.0)GO TO 88
        IF(VPN.LE.0)GO TO 88
        IF(TCN.LE.0)GO TO 88
72      CONTINUE
88      WRITE(2,47)
        WRITE(2,48)TCN,VPN,ASP,T
        STOP
        END
```
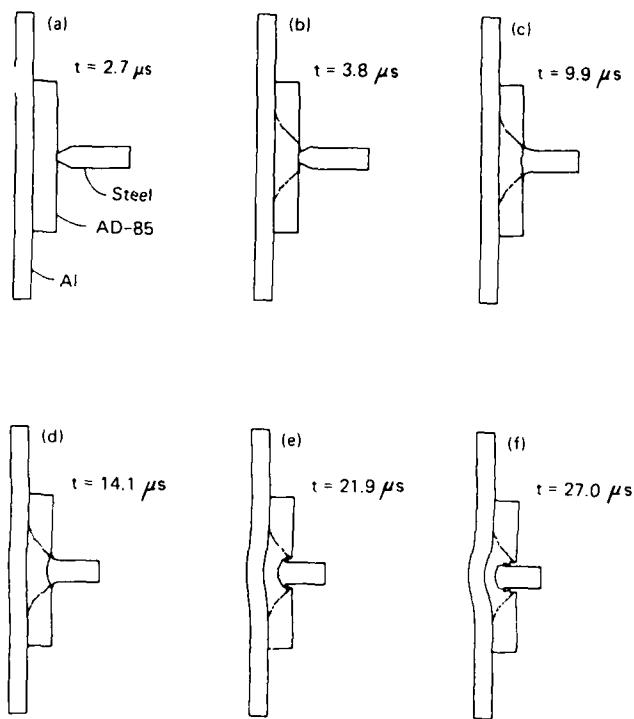
Figure 1 Computer simulation of the early stages of perforation of an 8.6 mm ceramic tile backed with 6.4 mm 6061-T6 aluminium by a projectile impacting at 853 ms^{-1}. The projectile erosion and formation of a fracture conoid in the ceramic are evident. After Wilkins [3].
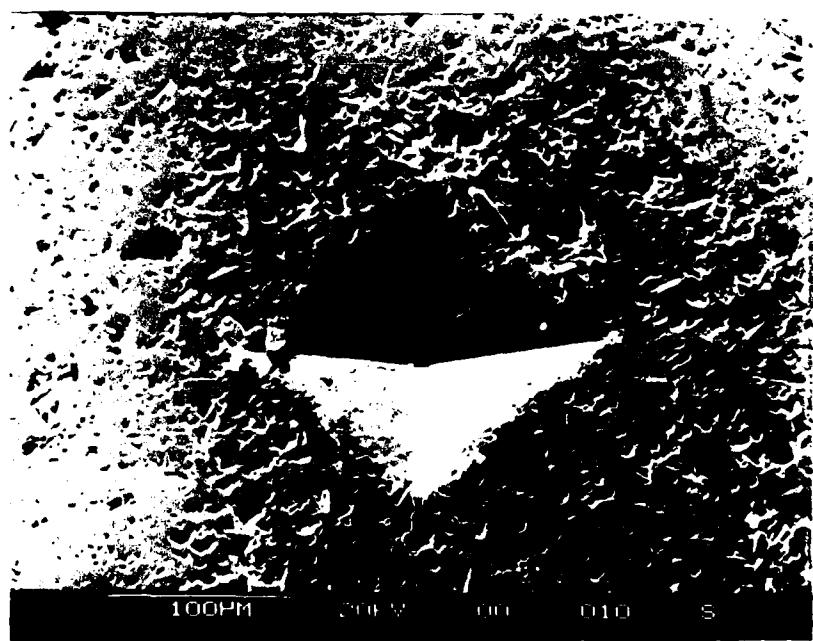
Figure 2 Typical Vickers diamond pyramid indentation into a ceramic.
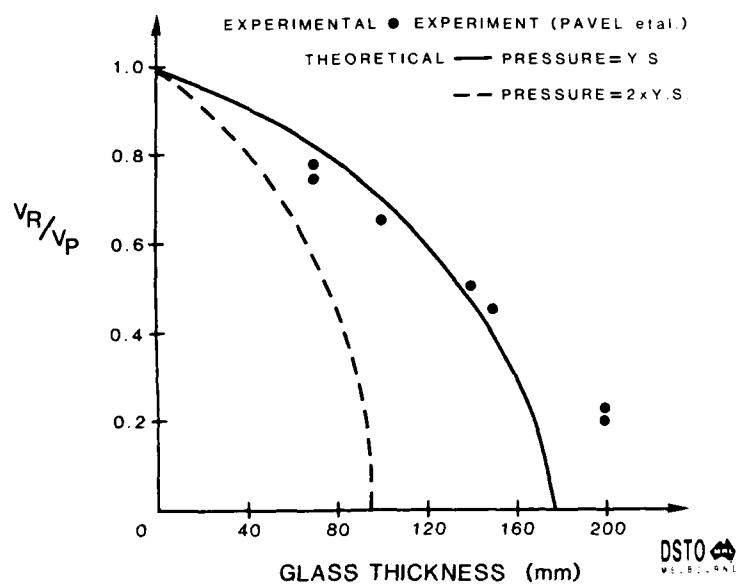
Figure 3   Calculations of the residual velocity/impact velocity ratio (V_R/V_P) for
            perforation of glass targets by non–deforming projectiles.   Two values of
            pressure resisting penetration are used and the experimental points are from
            Pavel et al. [15].

Ceramic

Hinge

Projectile
Erosion

Ductile
Backing

Ceramic
Erosion

Cone
Crack

(a)

Realistic

Model

$\dot{u}_T$

Velocity
Profile

(b)

M_P F_P ΔM_P F_I ΔM_C F_C M_T

F_T

Projectile

Target
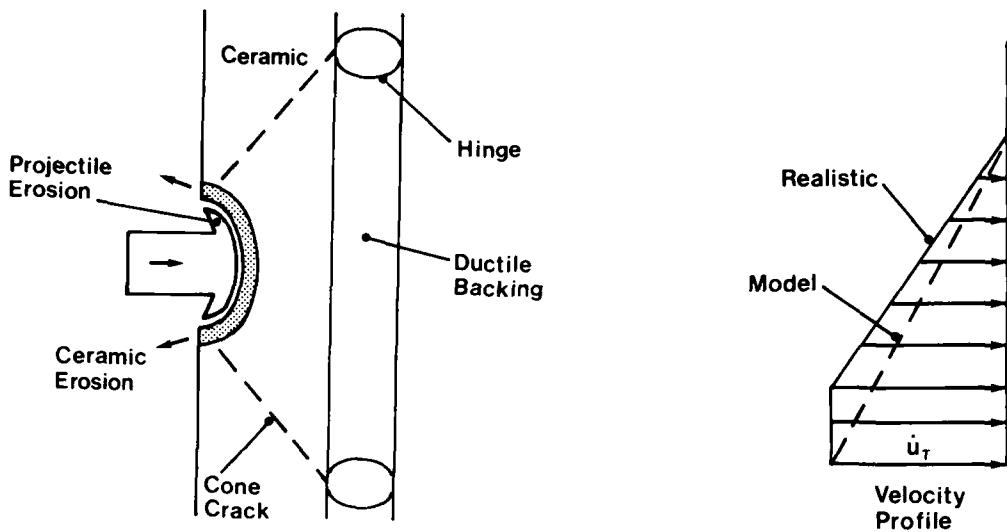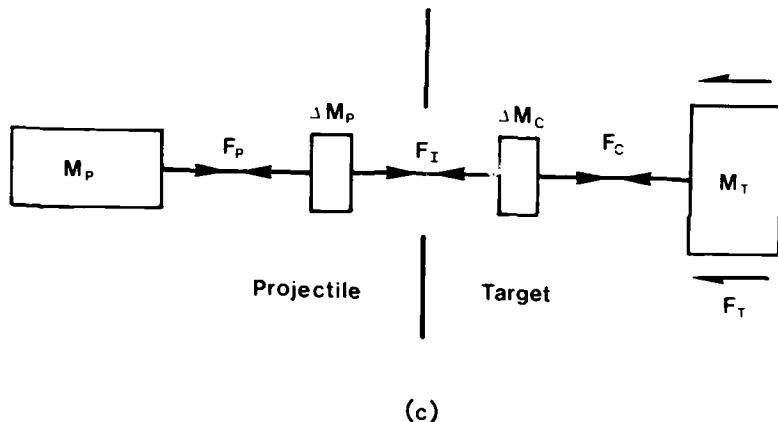
(c)

Figure 4   Basic concepts of the interaction of a penetrator with a ceramic tile backed
by a thin ductile plate. (a) Schematic of the eroding penetrator, eroding
ceramic material, cone crack and positions of the hinges for dishing of the
backing. (b) Assumed velocity distribution in the ceramic and backing
during the first stage of acceleration. The more realistic distribution has a
constant velocity from the axis to the projectile diameter, however a slightly
modified distribution was used in the model for computational simplicity.
(c) Lumped mass model, where the masses M and connecting forces F are
defined in the text. In a small time step masses ΔM_p and ΔM_c are eroded
from the projectile and ceramic respectively.
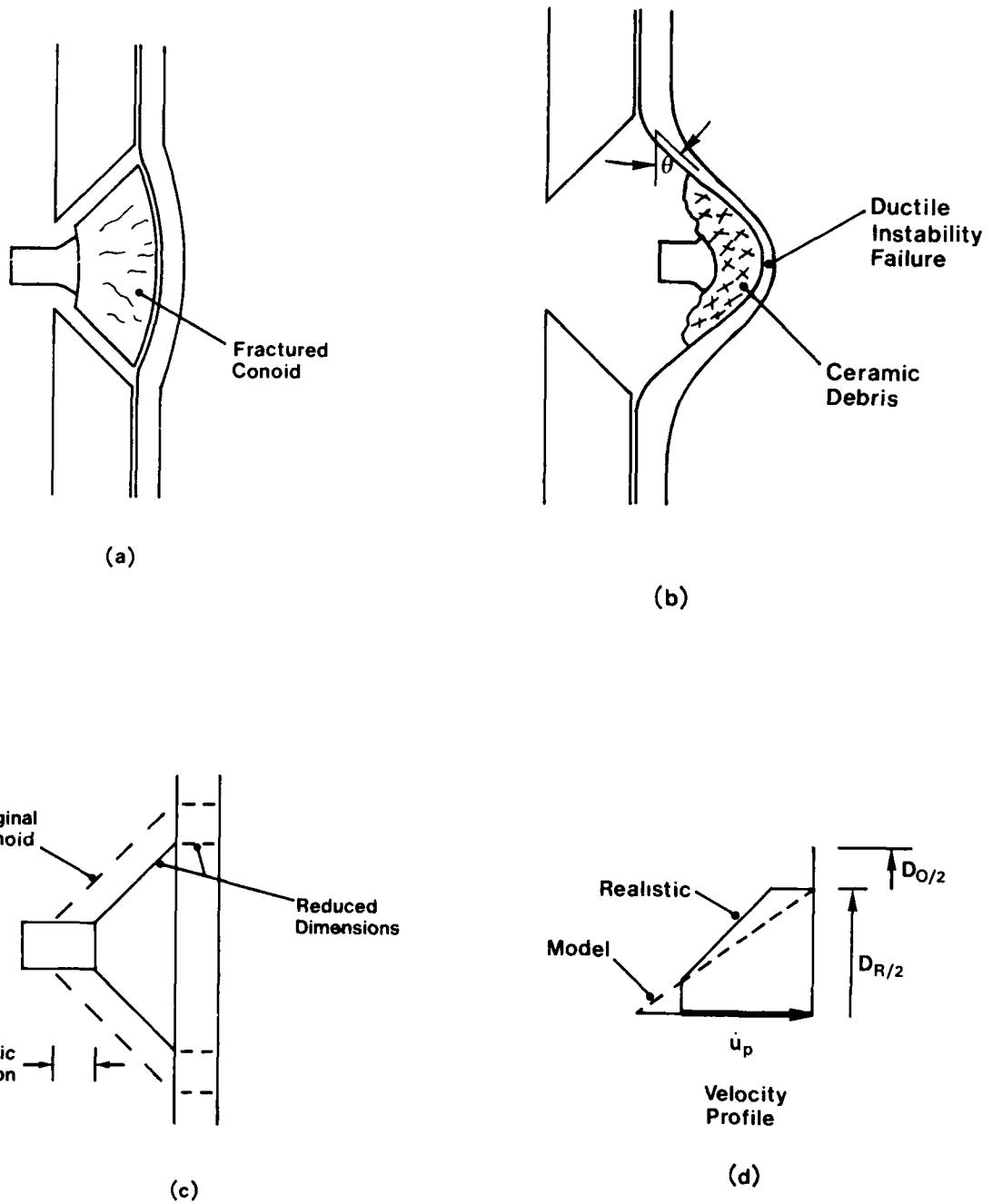
Figure 5   *Second stage of perforation of the ceramic tile with a thin backing where (a) the projectile, ceramic and backing move as a unit till (b) a biaxial tensile failure of the sheet occurs at an angle of bend θ.   (c) The assumed reduction in effective dimensions of the loaded conoid and backing plate as a result of ceramic erosion.   (d) Velocity distribution in the second stage where the more realistic distribution has a step near the reduced conoid outer diameter, but a simpler form is assumed for ease of computation.*
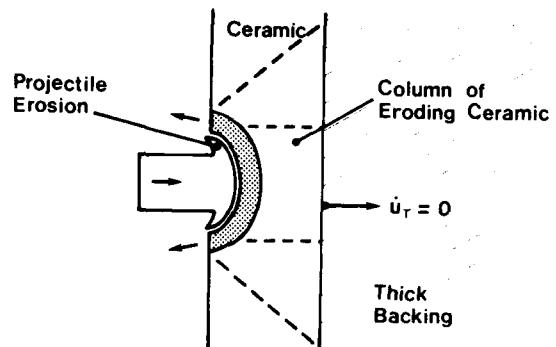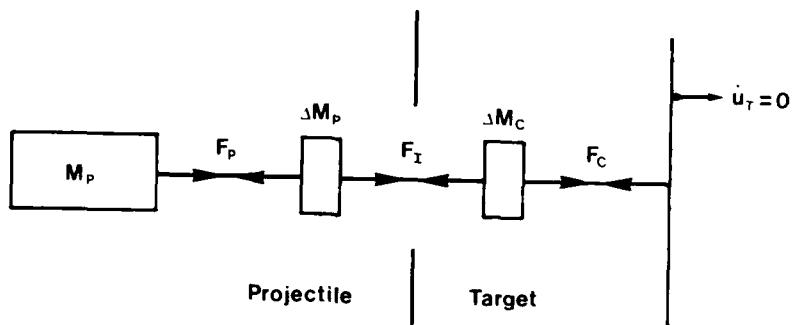
Figure 6   Model concept for the thick backing problem where it is assumed that the
backing remains effectively stationary whilst the ceramic is eroded.
(a) Schematic and (b) lumped mass model.
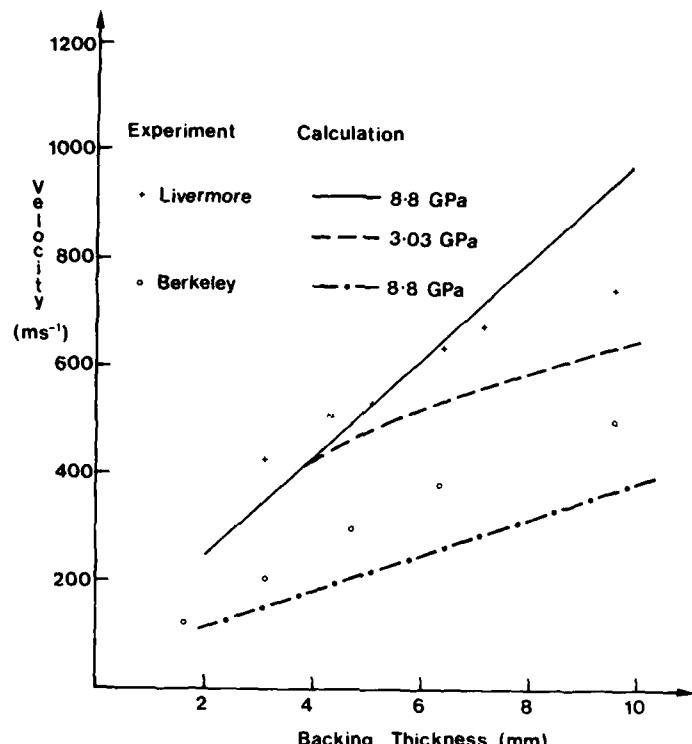
(a)
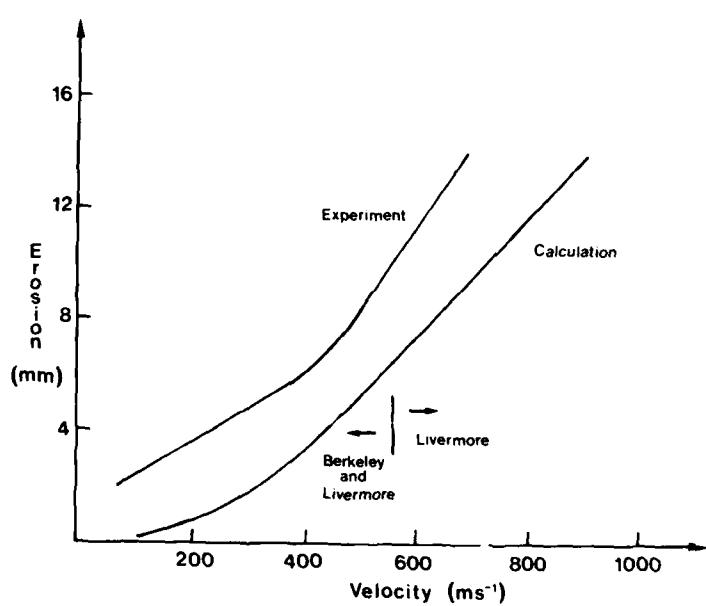
(b)

Figure 7   (a) Comparison of ballistic limit predictions using the model for thin
backings with data presented by Mayseless et al. [4].   For the Livermore
data, due to Wilkins [3], two values of ceramic strength have been used,
8.8 GPa corresponding to the hardness and 3.03 GPa corresponding to
hardness divided by 2.9.   (b) Comparison of penetrator erosion calculated
using the present model with the experimental curve of Mayseless et al. [4].
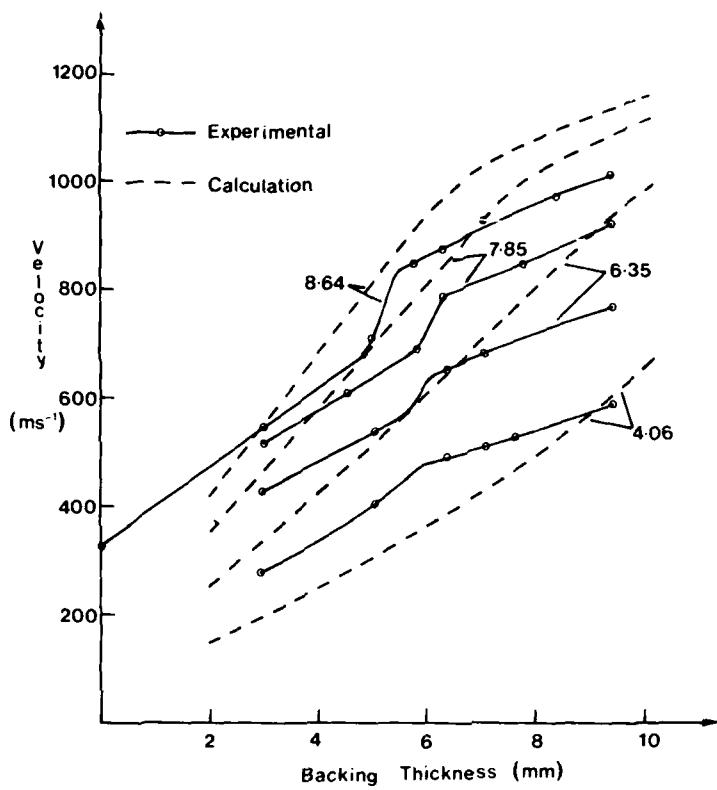
Figure 8   Comparison of ballistic limit computations with experimental data of Wilkins
[3] for four thicknesses of AD85 alumina ceramic and over a range of backing
thicknesses.
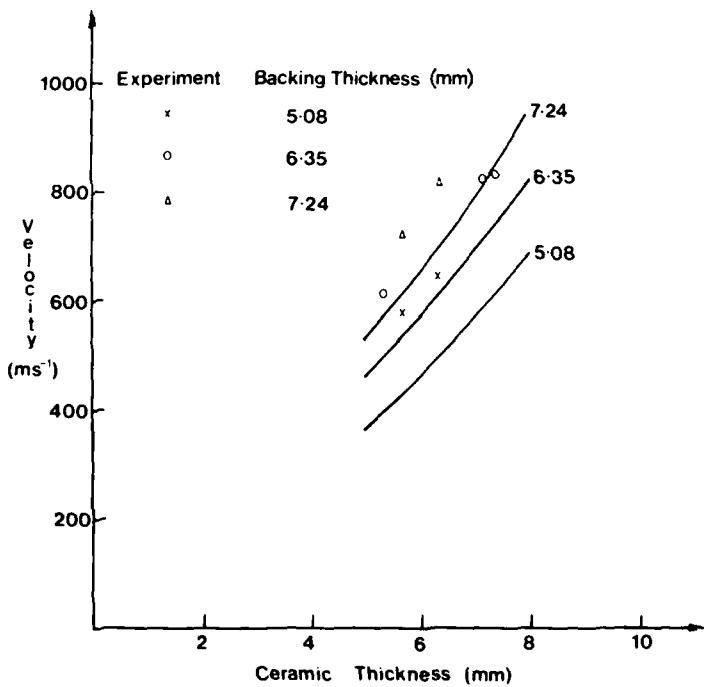
Figure 9   The comparison of model computations with experimental data of Wilkins
et al. [2] for aluminium backed boron carbide tiles.   Curves represent model
computations for the three backing thicknesses indicated.
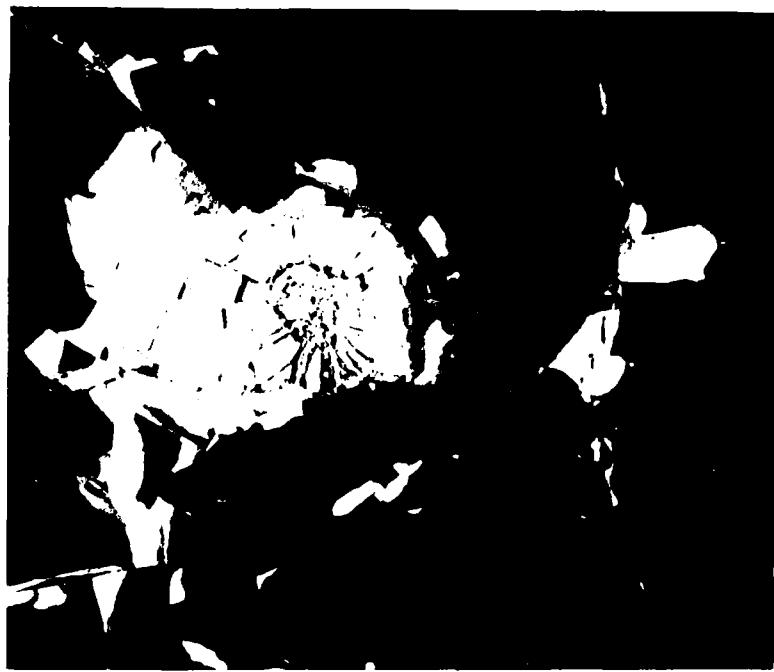
Figure 10   *An aluminium backed AD85 alumina target after impact by a steel cored armour piercing projectile below the ballistic limit, showing the radial and circumferential cracking and the maintenance of ceramic material between the projectile and the backing.*
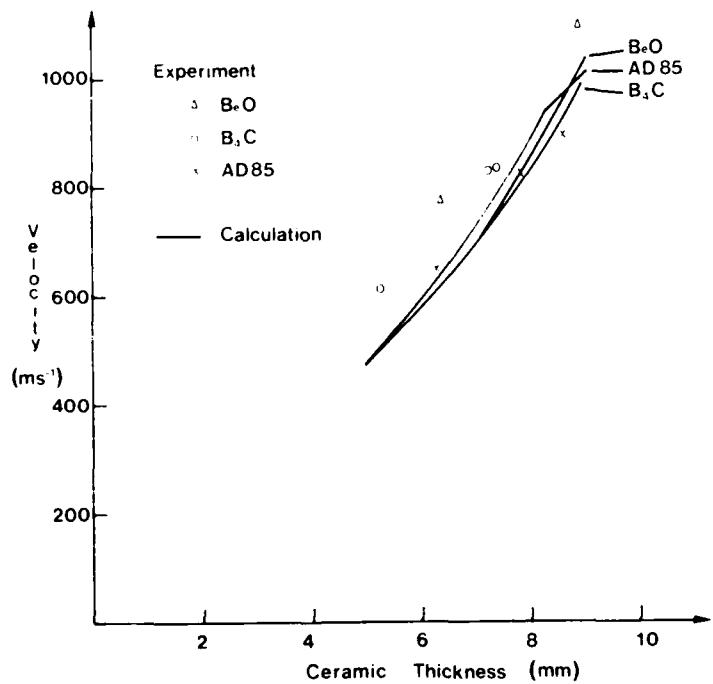

Figure 11   *Model computations compared to Wilkins et al. [2] empirical data for three different ceramic materials, beryllium oxide, AD85 alumina and boron carbide.*
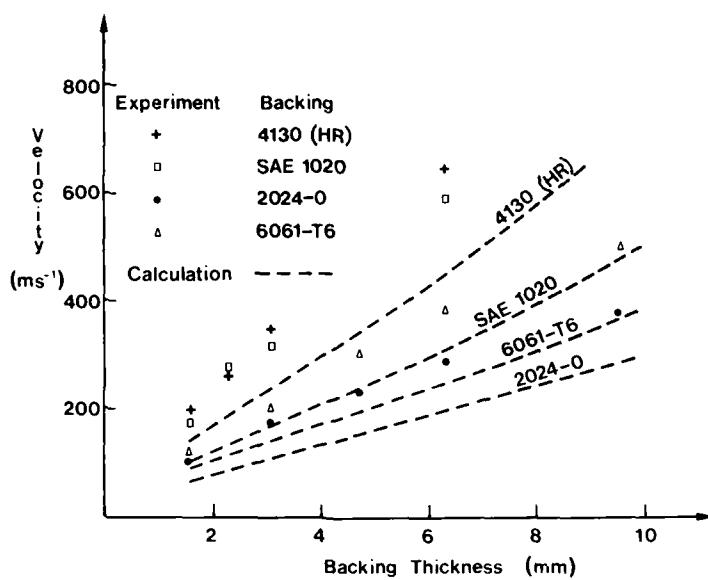
Figure 12   *The effect of backing material, comparing Mayseless et al. [4] empirical data for two steels, 4130 (HR) and 1020, and two aluminiums, 6061-T6 and 2024-O, with model calculations.*
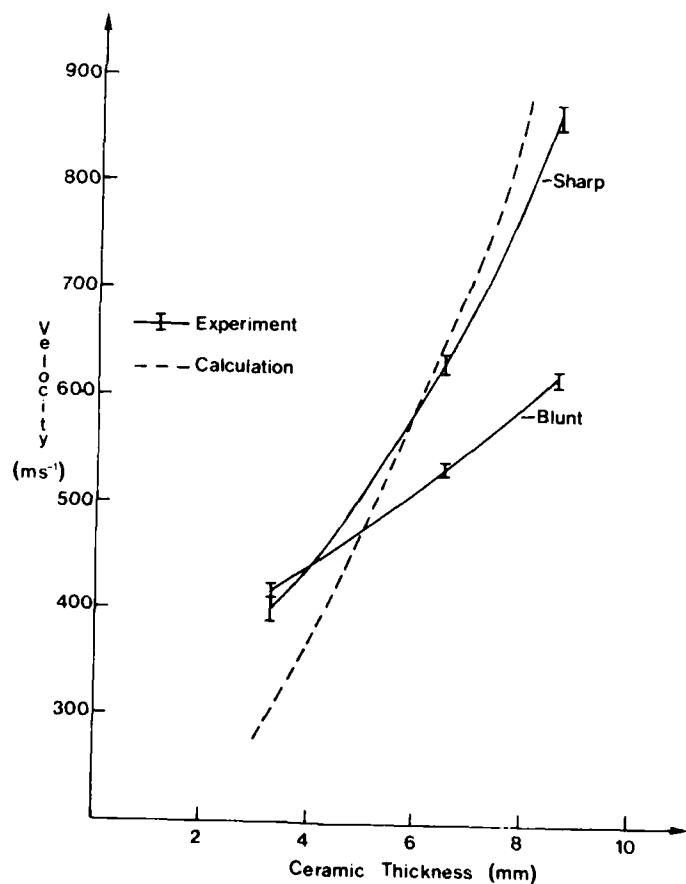

Figure 13   *Effect of projectile shape. The experimental data of Wilkins [1] is for sharp and for blunt penetrators, whilst the model computations assume a blunt penetrator.*
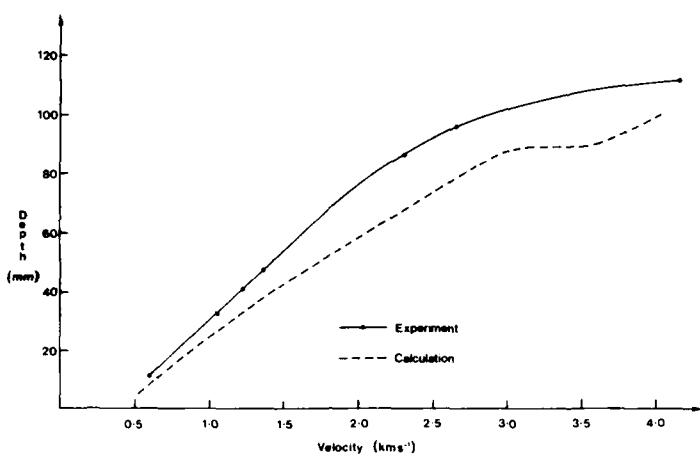
(a)
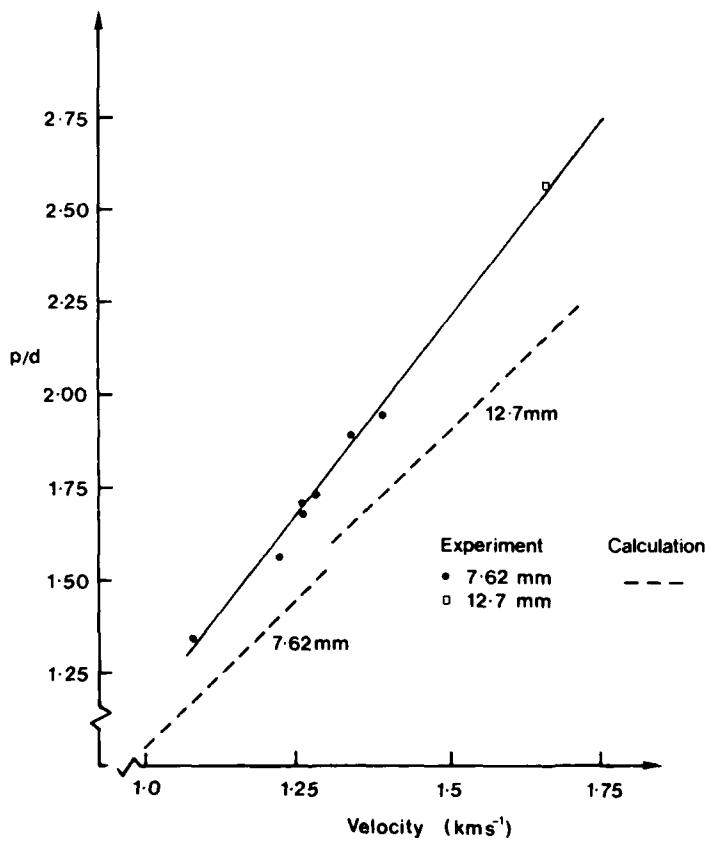
(b)

Figure 14   (a) *Depth of penetration as a function of impact velocity for tantalum rods comparing calculations using the deep penetration model [26, 27] with the empirical data of Bless et al. [28].*   (b) *Similar comparison for 7.62 mm and 12.7 mm fragment simulating projectiles.*
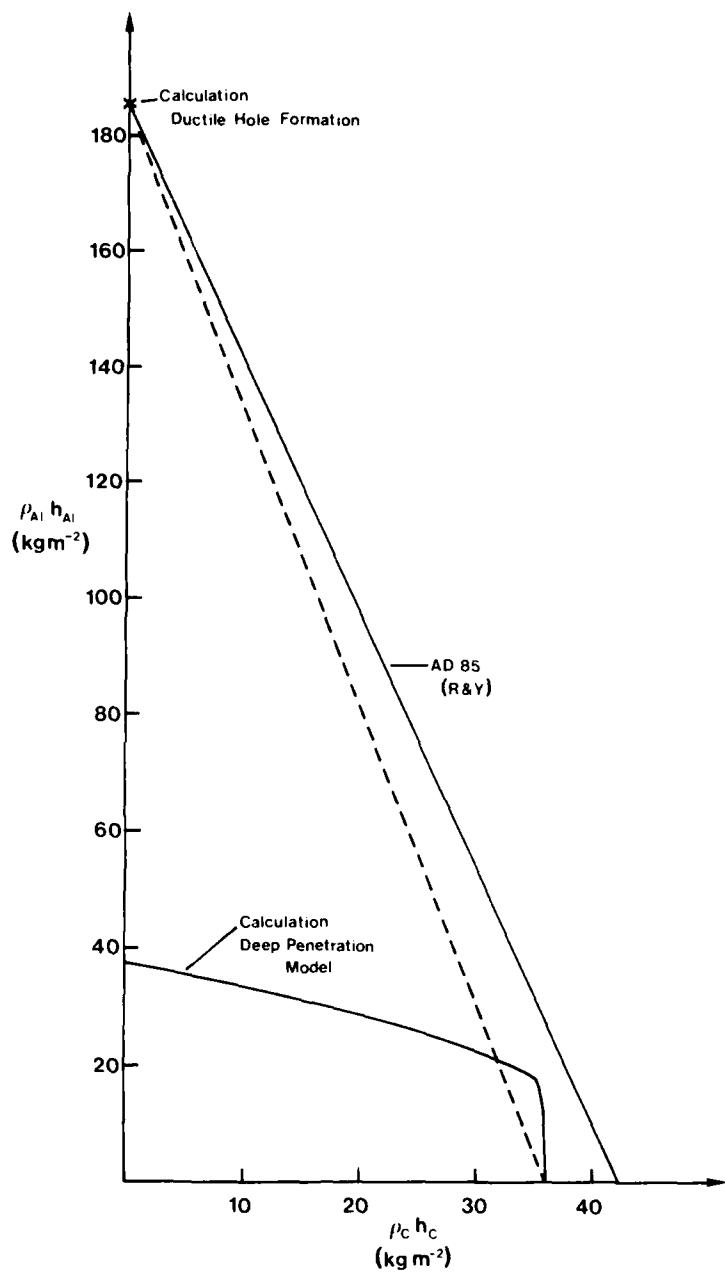
Figure 15   *Plot of $\rho_{Al} h_{Al}$ versus $\rho_c h_c$ as presented by Rosenberg and Yeshurun [5, 6]*
showing the experimental line for their AD85 data.   The calculated point for
penetration into bare aluminium using the ductile hole formation model
coincides with the experimental intercept on the ordinate.   Computations
with the thick backing model, ECS, combined with the deep penetration
model are used to establish an intercept on the abscissa using 5.6 GPa as the
AD85 alumina strength.   The two intercepts are joined to obtain a straight
line to compare with the empirical result.   Note that the effect of using a
blunt penetration compared to a sharp penetration model for the calculations
into bare aluminium, indicates that projectile blunting is the first major
influence of the ceramic on such hard penetrators.   It is evident that the
falling of experimental data on a straight line may only be approximate and
for low values of $\rho_{Al} h_{Al}$.

DOCUMENT CONTROL DATA SHEET

REPORT NO.	AR NO.	REPORT SECURITY CLASSIFICATION
MRL-RR-3-89	AR-005-713	Unclassified

TITLE

A basis for modelling ceramic composite armour defeat

AUTHOR(S)	CORPORATE AUTHOR
Raymond L. Woodward	DSTO Materials Research Laboratory PO Box 50 Ascot Vale Victoria 3032

REPORT DATE	TASK NO.	SPONSOR
June 1989	ARM 88/150	Army

FILE NO.	REFERENCES	PAGES
G6/4/8-3731	28	45

CLASSIFICATION/LIMITATION REVIEW DATE	CLASSIFICATION/RELEASE AUTHORITY
	Chief, Materials Division MRL

SECONDARY DISTRIBUTION

Approved for public release

ANNOUNCEMENT

Announcement of this report is unlimited

KEYWORDS

Composite armor	Lightweight armor	Fracture

SUBJECT GROUPS	0079B	0071B	0079E

ABSTRACT

This work takes some of the major features of ceramic composite armour failure, viz. fracture conoid formation, dishing failure of thin backing plates, perforation failure of thick backing plates, and projectile erosion, and by lumping masses to treat material acceleration simple models are developed which allow computations on ceramic targets with both thin and thick metallic backings. Two computer programs for these problems, CEP and ECS, are documented, and calculations compared with a broad range of empirical data and also used to discuss aspects of the interaction of penetrators with ceramic composite armours. The good correlation of models with experiment demonstrates the usefulness of the present approach for studying ceramic composite armour defeat.

END

FILMED

3-90

DTIC